Attomolar DNA Detection

DOI: 10.1002/anie.201006806

Label-Free Detection of Few Copies of DNA with Carbon Nanotube Impedance Biosensors**

*Tetiana Kurkina, Alexis Vlandas, Ashraf Ahmad, Klaus Kern, and Kannan Balasubramanian**

The detection of specific nucleic acid sequences plays a vital role in environmental, food, and clinical monitoring and in forensic screening.[1] The ability to detect few copies of DNA is expected to have a broad impact on the rapid on-site detection of various diseases.[2] In current methods, amplification of the sample through the use of the polymerase chain reaction (PCR) enables a detectable amount of DNA to be obtained.[3] For applications involving the comparison of gene expression levels, microarrays are used.[4] This approach requires the labeling of target sequences for subsequent detection with a fluorescence microscope. The need for PCR, labeling, and a bulky optical reading instrument limits the use of such sensors for point-of-care applications. New methods in which PCR or labeling steps could be avoided would be advantageous; furthermore, a portable, cost-effective sensing device is required.

Electrical methods are ideally suited for this purpose, since they do not require the target to be labeled and are compatible with a compact and portable format. Label-free electrical detection of DNA has been demonstrated in many configurations,[5] the majority of which are based on field-effect[6,7] or electrochemical detection.[8] Although the use of a label is avoided in these experiments, the limit of detection is comparable to that of optical methods; hence, an amplification step is also required. To improve the limit of detection, nanostructures have been proposed as suitable alternatives for active elements of biosensors.[9–11] One-dimensional nanostructures are promising candidates, since they can be used as active elements of field-effect transistors in a facile manner.[7,11–13] Furthermore, a 1D nanostructure, such as a single-walled carbon nanotube (CNT), has all atoms on its surface. Since every atom limits the current flowing through it, these structures show promise for absolute sensitivity. Alternative candidates, such as silicon nanowires (SiNWs), have also been the focus of extensive experimentation;[14–18] the lowest reported detection limit is 10 fM.[16,17] However, SiNWs suffer from extremely high resistance (in the gigaohm range), which limits the attainable sensitivity.[16] Almost all SiNW sensors are based on resistive detection without the use of a reference electrode. Although the lack of a reference electrode is useful in the demonstration of prototype sensors, the use of a reference electrode is unavoidable when stability and reproducibility of the sensors are required.[7,19,20]

On the basis of the lower diameter of CNTs and their superior conducting properties, we describe herein sensors with close to absolute sensitivity, with a detection limit two orders of magnitude lower than that reported for silicon nanowires.[16,17] The challenge that we have overcome is to achieve such a low detection limit while preserving the simplicity of electrical detection and the reproducibility of sensing characteristics. In comparison to field-effect sensors based on CNT networks,[21] our sensors show an improvement in the detection limit by up to five orders of magnitude. Another unique aspect of our nanosensors is that detection is performed directly in buffer solutions at a physiologically relevant ionic strength. Finally, we demonstrate the highly specific detection of attomolar DNA in a heterogeneous DNA mixture in which the target DNA comprises just 2% of the total DNA concentration.

Figure 1 shows an overview of the assembled carbon nanotube sensor. Details of the fabrication can be found in the Supporting Information. In short, a few (on average five) nanotubes are trapped across photolithographically prepared electrode gaps (3 μm; see Figure 1b). The electrodes are passivated with SiO_2, and only the CNTs are in contact with the solution. The liquid is delivered to the sensor chip through a microwell that is fixed on the chip (see Figure 1a). An Ag/AgCl reference electrode placed in the reservoir acts as the gate electrode.

For the detection of a specific target DNA sequence through hybridization, a complementary probe sequence needs to be immobilized on the nanotube surface. For this purpose we utilize a versatile electrochemical functionalization route that we have developed and used successfully to demonstrate a range of sensors based on nanotubes[22–24] and graphene.[25] The functionalization protocol for attachment of the probe sequence is shown in Scheme 1. First, 4-aminobenzoic acid (ABA) is electropolymerized onto the nanotube surface. This process results in the noncovalent[22,26] wrapping of the nanotubes with -COOH groups. In a second step, amino-functionalized probe DNA (24 base pairs) is covalently coupled to the -COOH groups through amide formation after activation with a carbodiimide. The nonfunctional-

[*] T. Kurkina, Dr. A. Vlandas, Dr. A. Ahmad, Prof. K. Kern, Dr. K. Balasubramanian
Max-Planck-Institut für Festkörperforschung
Heisenbergstrasse 1, 70569 Stuttgart (Germany)
Fax: (+49) 711-689-1662
E-mail: b.kannan@fkf.mpg.de
Prof. K. Kern
Institut de Physique de la Matière Condensée
Ecole Polytechnique Fédérale de Lausanne (Switzerland)

[**] This project was funded by the German Federal Ministry of Education and Research (BMBF, ID: O3X5516). We thank S. Schmid (Technology Group) for help with photoresists; V. Pachauri for SEM imaging; and Dr. K. Heimann (Karlsruhe Institute of Technology) and Prof. C. Richert (University of Stuttgart) for providing us with gold-nanoparticle-decorated DNA.

Supporting information for this article is available on the WWW under http://dx.doi.org/10.1002/anie.201006806.

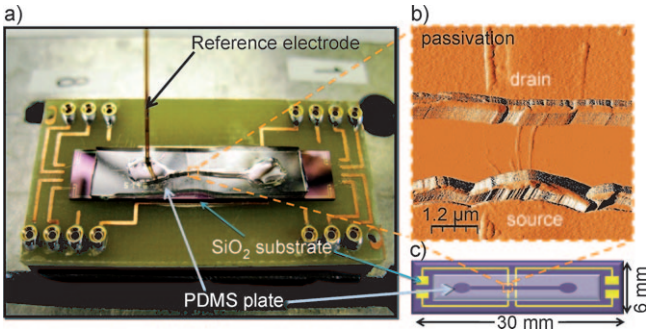

Figure 1. The CNT–DNA impedance biosensor. a) Photograph showing the chip carrier (printed circuit board) with the sensor chip covered with a poly(dimethylsiloxane) (PDMS) layer. The sensor chip is wire-bonded to the chip carrier, and the nanotubes are trapped across the gap between two platinum electrodes. The PDMS layer comprises two reservoirs connected by a microchannel and is shown filled with the buffer solution. The channel is positioned above the electrode gap. An Ag/AgCl reference electrode placed in one of the reservoirs is also visible. b) Atomic force microscope (AFM) image of the nanotubes trapped dielectrophoretically between passivated Pt electrodes. c) Schematic illustration of the sensor chip showing the position of the Pt electrode lines and the electrode gap.

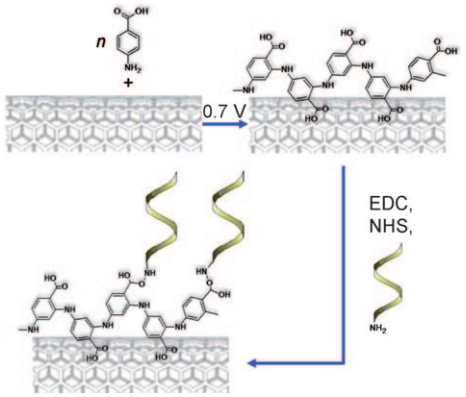

Scheme 1. Controlled functionalization of the carbon nanotube surface with probe DNA. First, 4-aminobenzoic acid is electropolymerized onto contacted nanotubes by applying +0.7 V versus Ag/AgCl. A polymer coating results with a thickness of 2–3 nm around the nanotubes. In a second step, 3′-NH_2-DNA is coupled to the carboxylic groups through amide formation by treatment with 1-ethyl-3-(3-dimethylaminopropyl)carbodiimide hydrochloride (EDC) and *N*-hydroxysuccinimide (NHS).

ized sections are subsequently blocked with ethanolamine. The height increase upon electropolymerization was estimated from AFM images to be around 2–3 nm.

Our electrochemical functionalization approach is unique and offers a number of key advantages. First, the functionalization is site-specific; that is, only the nanotubes addressed by the electrochemical modification are preferentially decorated with probe DNA. The site specificity of functionalization also ensures that there is no DNA in the vicinity of the nanotubes on the chip surface. In contrast, if spotting is used, the DNA can be immobilized anywhere in the spotting area,[21,27] and a high level of background noise can result, as commonly observed in microarray detection.[4,28] Furthermore, the negatively charged carboxylic groups are expected to minimize direct nonspecific binding of DNA on the nanotube surface occurring due to hydrophobic interactions.[29] These aspects are pivotal in the attainment of the attomolar detection limit in our nanoscale sensors.

The sensing trials were performed at varying concentrations of target DNA (24 base pairs) in 10 mM potassium phosphate buffer containing 0.1 M NaCl. The impedance of the nanotube (Z, a complex quantity with a magnitude and a phase) constitutes the sensor response, which is measured in the frequency range between 20 Hz and 2 MHz.[22] The frequency response is measured at varying gate voltages to characterize the field-effect behavior. The resulting dataset can be visualized in the form of a 2D magnitude Z-map and a 2D phase Z-map (Figure 2).

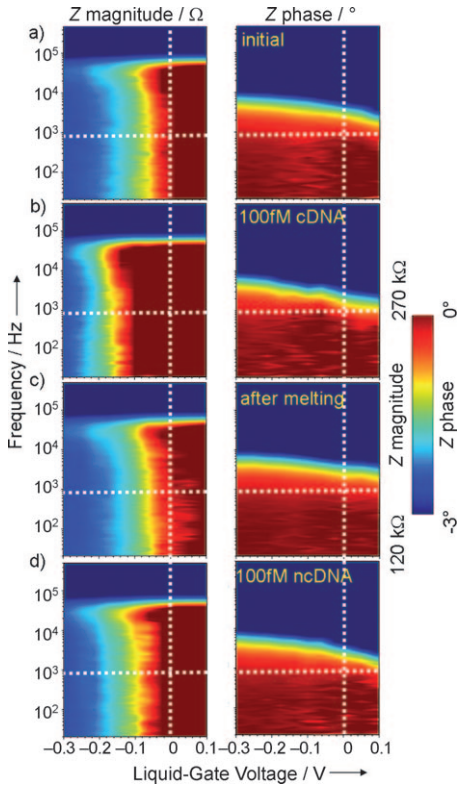

Figure 2. Specificity of the CNT–DNA sensors. The plots show magnitude Z-maps (left column) and phase Z-maps (right column) for different buffer solutions: a) without target DNA; b) with complementary target DNA (cDNA); c) after melting and washing; d) with non-complementary DNA (ncDNA). It is apparent that for cDNA (b), the sensor response shifts to the left, whereas this change is minimal for ncDNA (d). The maximum response time is 30 min.

We first discuss the sensor response of the fabricated devices to target DNA (100 fM) in buffer (Figure 2). The Z-magnitude and Z-phase maps were first recorded in the buffer solution without any target DNA. The resistance of the device is around 100–300 kΩ, which is dominant at low frequencies. In this range, the device impedance exhibits a low gate modulation. At high frequencies, capacitive components

arising from both the electrical double layer and the substrate dominate (Figure 2a). Upon the addition of complementary target DNA to the microwell, the *Z*-magnitude response shifts to the left (Figure 2b) along the gate-voltage scale (*x* axis). The *Z*-phase response shows differences in the frequency range 1–10 kHz. After melting of the hybridized strand and subsequent washing, the initial response is recovered (Figure 2c). To confirm that the signal is indeed due to specific hybridization of the complementary target, we measured the sensor response upon the introduction of a 3 bp-mismatched noncomplementary sequence at the same concentration (Figure 2d). The *Z*-maps shift only slightly in this case.

To understand the sensor response, it is worth taking a closer look at the specificity of the sensor characteristics. In the presence of the complementary target, the magnitude as well as the phase response (Figure 2; see also Figure S1 in the Supporting Information) are shifted to negative gate voltages. The device functions like an ion-sensitive field-effect transistor (ISFET), whereby changes in the surface charge lead to a shift in the threshold voltage. This threshold shift of around 120 mV can be attributed to the accumulation of negative charges on the nanotube surface upon hybridization. The sign of the threshold shift is consistent with data reported on DNA sensors based on nanotube networks.[27] Upon melting and subsequent washing of the sensor surface, the negative charges of the complementary strand are removed, and the sensor response returns to the initial scenario. The sensor response for the 3-bp-mismatched DNA shows only a comparatively negligible shift (less than 20 mV to the left) signifying a much lower degree of hybridization, as is normally expected for a mismatched DNA sequence.[30] We performed a number of control experiments to ensure that the changes arise exclusively from hybridization of the target strands with the attached probe sequences (see the Supporting Information).

The use of high-frequency detection ensures very low noise. This coupled with the stable Ag/AgCl reference electrode provides for excellent stability. These features enable repetitive use of the same sensor for a series of DNA samples at different concentrations with minimal drift. Figure 3 shows the concentration dependence of the sensor response for one of the devices in the form of magnitude *Z*-maps (Figure 3a) and phase *Z*-maps (Figure 3b) for various concentrations of complementary target DNA. Section profiles extracted from the maps in Figure 3a are collected in Figure 4a. It is apparent that the gate response shifts to more negative gate voltages as the concentration of target DNA increases. The calibration curves in Figure 4b are plots of the shift in threshold voltage as a function of DNA concentration for both the target (cDNA) and the noncomplementary sequence (ncDNA). It is apparent that the sensor response for cDNA is linear over a broad concentration range. It is clearly stronger and distinct from that of ncDNA. A target concentration as low as 100 aM can be detected unambiguously with high specificity. This concentration corresponds to around 1800 molecules of target DNA in our 30 μL sample droplet in the microwell and is the lowest detectable concentration that

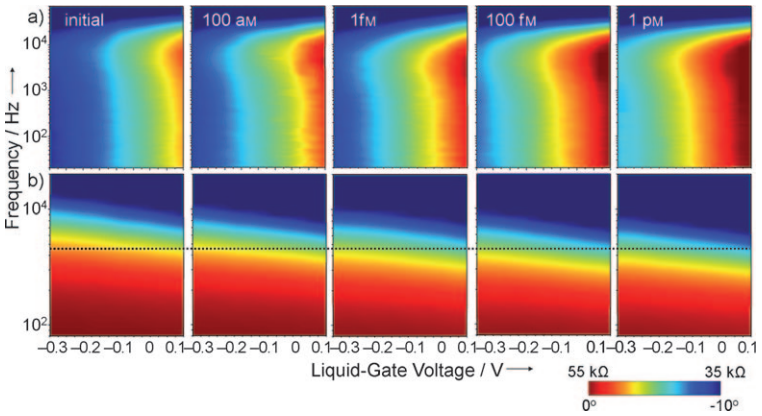

Figure 3. Attomolar detection limit of the CNT–DNA sensor. a) Magnitude *Z*-maps and b) phase *Z*-maps for various concentrations of complementary target DNA. After each exposure of the sensor to target DNA, the hybrids were melted to return the sensor to its initial state, as shown in Figure 2a–c. It is apparent that even at a cDNA concentration of 100 aM (corresponding to around 1800 molecules in our 30 μL droplet), the sensor response can be discerned unambiguously. Thus, an ultralow detection limit is attainable with the CNT impedance biosensors.

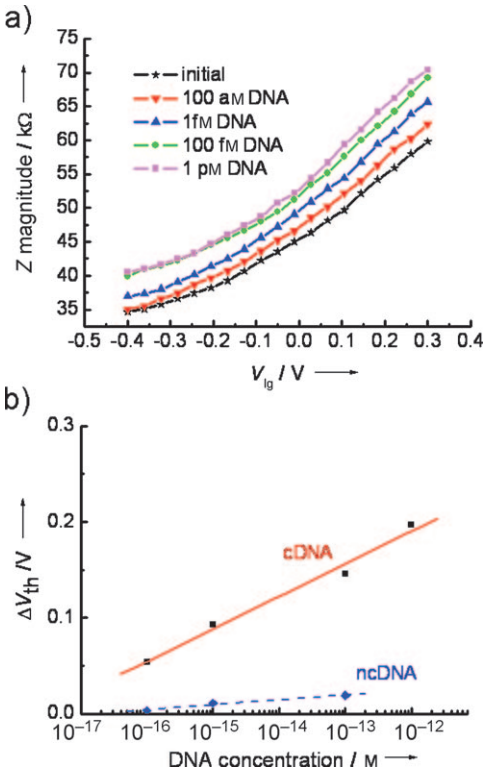

Figure 4. Sensitivity of the CNT–DNA sensor. a) Gate dependence of the magnitude of impedance at a frequency of 1 kHz in buffer solution (black line) and for varying concentrations of complementary target DNA (cDNA) in buffer solution (extracted from Figure 3a). The threshold voltage shifts to more negative voltages as the cDNA concentration increases. b) Calibration curve showing the threshold shift as a function of DNA concentration for both cDNA and noncomplementary (ncDNA) sequences. It is apparent that the response for cDNA is linear and is clearly distinct from that of ncDNA.

has been reported for any label-free or mediator-free direct detection technique.

As mentioned earlier, the ability to detect few copies of the target DNA is made possible primarily by ensuring that the high surface-to-volume ratio is guaranteed through appropriate passivation of the electrodes, which leaves exclusively the nanotube surface as the active element. Furthermore, the low resistance, the stability gained by the use of the impedance measurement, and the site-specific electrochemical functionalization route were key to the achievement of this ultralow detection limit. These ultrasensitive sensors were created simply by photolithography, without the need for any expensive serial technique, such as electron-beam lithography. In combination with the dielectrophoretic trapping procedure, our fabrication protocol is a scalable method for the routine generation of ultrasensitive nanoscale DNA sensors.

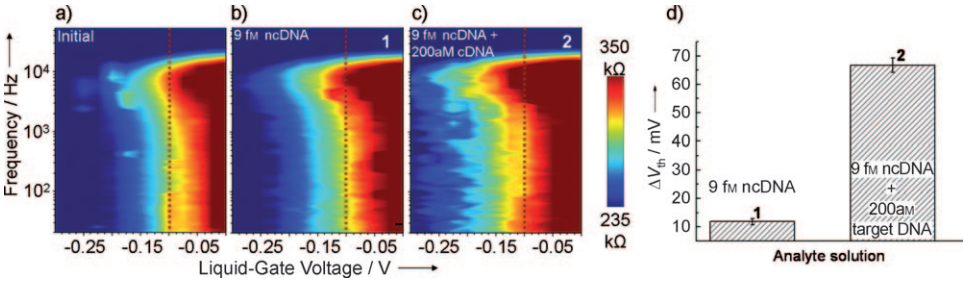

Figure 5. Attomolar target differentiation in a heterogeneous DNA mixture. Magnitude *Z*-maps measured in a) the buffer solution, b) a heterogeneous mixture of three different noncomplementary sequences (ncDNA), each at a concentration of 3 fM (total DNA concentration: 9 fM) in buffer solution, and c) in the mixture in (b) with complementary target DNA (cDNA; 200 aM) added. d) Sensor signal (threshold shift) for the mixtures in (b) and (c). In the mixture with cDNA, the complementary target amounts to just 2% of the total DNA. The CNT–DNA sensor is capable of differentiating this small amount from the noncomplementary background present at a much higher concentration of 9 fM. Thus, the sensor shows high selectivity coupled with an ultralow detection limit.

To evaluate the use of our nanobiosensors in a realistic application scenario, we validated our analytical strategy for the specificity of DNA differentiation at ultralow concentrations. For this purpose, we took a heterogeneous mixture of three different ncDNA sequences (noncomplementary to the probe sequence), each at a concentration of 3 fM, and added complementary DNA (cDNA; 200 aM) to give a total DNA concentration of 9.2 fM. The amount of cDNA that we were aiming to detect corresponded to only around 2% of the total DNA in the mixture. As a control, we used the ncDNA mixture without the cDNA at a total DNA concentration of 9 fM. Figure 5 shows the *Z*-maps measured in buffer, in the ncDNA control, and in the ncDNA/cDNA mixture. A significant shift to the left, as in Figure 3, was only observed if the buffer solution contained the complementary target (Figure 5c). This distinction is further clear from the threshold-voltage shifts summarized in Figure 5d for the heterogeneous samples with and without the cDNA. It is apparent that cDNA at a concentration of 200 aM and comprising just 2% of the heterogeneous sample was able to generate a significant threshold shift of around 65 mV. On the other hand, the 9 fM ncDNA control solution without the cDNA only showed a shift of around 12 mV, which is below the 20 mV shift expected to occur as a result of nonspecific interactions (as mentioned earlier). The power of our nanosensors is apparent from these measurements and gives reason to hope that the technique can be extended to the direct detection of low quantities of DNA in realistic biological samples, such as serum (after preprocessing). Ultimately, we hope that it will be possible to use the technique in a clinical setting without amplification or labeling steps.

In conclusion, we have described a robust and routine method for the fabrication of carbon nanotube impedance biosensors for the ultrasensitive detection of DNA. With the ability to detect a few thousand molecules in the sample solution, our method raises hopes for attaining the capability to detect individual molecules. Another key advantage of our technique is its sensitivity in realistic and practical buffer solutions and heterogeneous environments, which are crucial for the recognition of molecular recognition events.[18] However, a number of key points still remain to be demonstrated. The experiments were conducted with synthetic oligonucleotides. It will be important to investigate the sensitivity of this method with real nucleic acid sequences from biological samples. We have set the basis for such future experiments. Given the scalability of our cost-effective method in combination with the lack of labeling and the high sensitivity, the emergence of on-chip nanobiosensors is expected to have a broad impact on a variety of diagnostic applications in the life sciences.

Received: October 29, 2010
Revised: February 7, 2011
Published online: March 18, 2011

Keywords: carbon nanotubes · DNA assays · electrochemical functionalization · impedance biosensors · nanobiosensors

[1] J. Sklar, *Hum. Pathol.* **1985**, *16*, 654–658.
[2] "Gene Expression by mRNA Analysis": J. H. Paul, H. P. John, *Methods in Microbiology*, *Vol. 30*, Academic Press, New York, **2001**, pp. 395–408.
[3] "Advances in Real Time PCR: Application to Clinical Laboratory Diagnostics": B. Kaltenboeck, C. Wang, S. M. Gregory, *Advances in Clinical Chemistry*, *Vol. 40*, Elsevier, Amsterdam, **2005**, p. 219.
[4] "DNA Microarrays in Biological Discovery and Patient Care": A. J. Yee and S. Ramaswamy in *Genomic and Personalized Medicine*, *Vol. 1* (Eds.: H. F. Willard, G. S. Ginsburg), Academic Press, New York, **2009**, p. 157.
[5] F. Yan, H. Tang, *Expert Rev. Mol. Diagn.* **2010**, *10*, 547–549.
[6] G. Gruner, *Anal. Bioanal. Chem.* **2006**, *384*, 322–335.
[7] K. Balasubramanian, *Biosens. Bioelectron.* **2010**, *26*, 1195–1204.

[8] T. G. Drummond, M. G. Hill, J. K. Barton, *Nat. Biotechnol.* **2003**, *21*, 1192 – 1199.
[9] K. Balasubramanian, M. Burghard, *Anal. Bioanal. Chem.* **2006**, *385*, 452 – 468.
[10] A. K. Wanekaya, W. Chen, N. V. Myung, A. Mulchandani, *Electroanalysis* **2006**, *18*, 533 – 550.
[11] S. Roy, Z. Gao, *Nano Today* **2009**, *4*, 318 – 324.
[12] K. Balasubramanian, E. J. H. Lee, R. T. Weitz, M. Burghard, K. Kern, *Phys. Status Solidi A* **2008**, *205*, 633 – 646.
[13] B. He, T. J. Morrow, C. D. Keating, *Curr. Opin. Chem. Biol.* **2008**, *12*, 522 – 528.
[14] Y. L. Bunimovich, Y. S. Shin, W.-S. Yeo, M. Amori, G. Kwong, J. R. Heath, *J. Am. Chem. Soc.* **2006**, *128*, 16323 – 16331.
[15] N. Elfström, R. Juhasz, I. Sychugov, T. Engfeldt, A. Eriksson Karlström, J. Linnros, *Nano Lett.* **2007**, *7*, 2608 – 2612.
[16] Z. Gao, A. Agarwal, A. D. Trigg, N. Singh, C. Fang, C.-H. Tung, Y. Fan, K. D. Buddharaju, J. Kong, *Anal. Chem.* **2007**, *79*, 3291 – 3297.
[17] J. Hahm, C. M. Lieber, *Nano Lett.* **2004**, *4*, 51 – 54.
[18] E. Stern, R. Wagner, F. J. Sigworth, R. Breaker, T. M. Fahmy, M. A. Reed, *Nano Lett.* **2007**, *7*, 3405 – 3409.
[19] L. Larrimore, S. Nad, X. Zhou, H. Abruna, P. L. McEuen, *Nano Lett.* **2006**, *6*, 1329 – 1333.
[20] E. D. Minot, A. M. Janssens, I. Heller, H. A. Heering, C. Dekker, S. G. Lemay, *Appl. Phys. Lett.* **2007**, *91*, 093507.
[21] A. Star, E. Tu, J. Niemann, J.-C. P. Gabriel, C. S. Joiner, C. Valcke, *Proc. Natl. Acad. Sci. USA* **2006**, *103*, 921 – 926.
[22] A. Vlandas, T. Kurkina, A. Ahmad, K. Kern, K. Balasubramanian, *Anal. Chem.* **2010**, *82*, 6090 – 6097.
[23] A. Maroto, K. Balasubramanian, M. Burghard, K. Kern, *ChemPhysChem* **2007**, *8*, 220 – 223.
[24] U. Schlecht, K. Balasubramanian, M. Burghard, K. Kern, *Appl. Surf. Sci.* **2007**, *253*, 8394 – 8397.
[25] R. S. Sundaram, C. Gómez-Navarro, K. Balasubramanian, M. Burghard, K. Kern, *Adv. Mater.* **2008**, *20*, 3050 – 3053.
[26] K. Balasubramanian, M. Burghard, *J. Mater. Chem.* **2008**, *18*, 3071 – 3083.
[27] E. L. Gui, L.-J. Li, K. Zhang, Y. Xu, X. Dong, X. Ho, P. S. Lee, J. Kasim, Z. X. Shen, J. A. Rogers, S. G. Mhaisalkar, *J. Am. Chem. Soc.* **2007**, *129*, 14427 – 14432.
[28] L. Bubendorf, *Eur. Urol.* **2001**, *40*, 231 – 238.
[29] M. Zheng, A. Jagota, E. D. Semke, B. A. Diner, R. S. Mclean, S. R. Lustig, R. E. Richardson, N. G. Tassi, *Nat. Mater.* **2003**, *2*, 338 – 342.
[30] G.-J. Zhang, G. Zhang, J. H. Chua, R.-E. Chee, E. H. Wong, A. Agarwal, K. D. Buddharaju, N. Singh, Z. Gao, N. Balasubramanian, *Nano Lett.* **2008**, *8*, 1066 – 1070.

